# APPLICATION OF HOMOGENOUS TRANSFORMATION MATRIX TO THE MODELING OF A BALL-END CUTTER

Jung-Fa Hsieh
*Far East University Department of Mechanical Engineering Tainan, 744, Taiwan*
*E-mail: seznof@cc.feu.edu.tw*

ICETI 2012-J1101_SCI
No. 13-CSME-63, E.I.C. Accession 3521

## ABSTRACT
This paper presents a comprehensive and straightforward method for the mathematical modeling of a generic ball-end cutter. In the proposed approach, a mathematical model of the rake surface is developed based on a normal helix cutting edge geometric model. A mathematical model of the flank surface is then derived based on the assumption of a constant clearance angle. The proposed model is applicable to a wide range of ball-end cutters. As a result, it provides an ideal basis for the generation of the NC equations required to machine ball-end cutters on a 6-axis CNC grinding machine.

**Keywords:** ball-end cutter; homogenous coordinate transformation; mathematical model.

# APPLICATION D'UNE MATRICE DE TRANSFORMATION HOMOGÈNE À LA MODÉLISATION D'UNE FRAISE À EMBOUT SPHÉRIQUE

## RÉSUMÉ
Cet article présente une méthode simple et complète pour la modélisation mathématique d'une fraise à embout sphérique génétique. Dans l'approche proposée, un modèle mathématique de la surface de la rainure est développé en se basant sur un modèle géométrique de l'angle de coupe d'une hélice normale. Un modèle mathématique de la surface du flanc est alors dérivé en se basant sur la présomption d'un angle de dégagement constant. Le modèle proposé est applicable à une grande variété de fraise à embout sphérique. De ce fait, il donne une base idéale pour la génération des équations NC requises pour les fraises à embout sphérique sur une machine à meuler CNC.

**Mots-clés :** fraise à embout sphérique ; homogène ; transformation coordonnée ; modèle mathématique.

## NOMENCLATURE

| | |
|---|---|
| ${}^{j}A_i$ | Configuration of frame $(xyz)_i$ with respect to frame $(xyz)_j$ |
| $\theta, \varphi$: | Parameters of ball surface |
| $R$: | Radius of ball-end cutter |
| $R_1$ | Radius of larger end face of conical type grinding wheel |
| $p_z$ | Lead of the helicoids of ball-end cutter |
| $\beta_0$ | Helix angle of cutting edge on cylindrical surface of ball-end cutter |
| $\beta$ | Helix angle of cutting edge on ball surface of ball-end cutter |
| $\rho$ | Semi-conical angle of grinding wheel |
| $H$ | Thickness of grinding wheel |
| $\lambda$ | Cutting edge inclination angle |
| $p_r$ | Tool reference plane |
| $\gamma_n$ | Normal rake angle |
| $\kappa_r$ | Cutting edge angle |

## 1. INTRODUCTION

Ball-end cutters are widely used for the machining of free-form surfaces and have therefore attracted significant attention in the literature. For example, Milfellner [1] performed a numerical investigation into the cutting forces developed in ball-end milling, while Lu et al. [2] presented an integrated methodology for the design, creation and evaluation of ball-end cutters. Jin et al. [3] developed a CBN ball-nosed end mill with a newly-designed cutting edge. Xiong and Bin [4] proposed a method for the CNC grinding of taper ball-end cutters using a torus-shaped grinding wheel. Chen and Bin [5] presented a novel method for producing the rake face of a taper ball-end mill using a CBN spherical grinding wheel. Chen et al. [6] performed a numerical investigation into the grinding of ball-end milling cutters with a constant normal rake angle. The current study presents a systematic methodology for modeling a ball-end cutter comprising a rake face with a constant normal rake angle and a flank face with a constant orthogonal clearance.

In the homogeneous coordinate transformation notation used in the present study, the point vector $a_x\mathbf{i} + a_y\mathbf{j} + a_z\mathbf{k}$ is written in the form of the column matrix ${}^{j}a = [a_x \;\; a_y \;\; a_z \;\; 1]^T$, where the pre-superscript "$j$" of the leading symbol indicates that the vector is defined with respect to coordinate frame $(xyz)_j$. Furthermore, given a point ${}^{j}a$, its transformation, ${}^{k}a$, is represented by the matrix product ${}^{k}a = {}^{k}A_j^{j}a$, where ${}^{k}A_j$ is a $4 \times 4$ matrix defining the position and orientation. Note that the same notation rules are also applied to the unit directional vector, i.e. ${}^{j}\mathbf{n} = [\mathbf{n}_x \;\; \mathbf{n}_y \;\; \mathbf{n}_z \;\; 0]^T$.

## 2. CUTTING EDGE OF BALL-END CUTTER

This section derives a model for the ideal cutting edge curve of a ball-end cutter. The cutting edge curve (see Fig. 1) can be expressed as

$$\mathbf{r} = [r_x \;\; r_y \;\; r_z \;\; 1]^T = [RC\theta C\varphi \;\; RC\theta S\varphi \;\; RS\theta \; 1]^T, \tag{1}$$

where $C$ and $S$ denote cosine and sine, respectively. $R$ is the radius of the ball surface.

The variation of a helical edge curve is generally expressed as a function of the helix angle, $\beta$. For the case of orthogonal helicoids, the cutting edge can be expressed as

$$\mathbf{r} = [r_x \;\; r_y \;\; r_z \;\; 1]^T = \left[R_Z C\varphi \;\; R_Z S\varphi \;\; \frac{p_z}{2\pi}\varphi 1\right]^T, \tag{2}$$

where $p_z$ is the pitch of the helix.

From Eqs. (1) and (2), the following relationship is obtained:

$$S\theta = k\varphi, \tag{3}$$

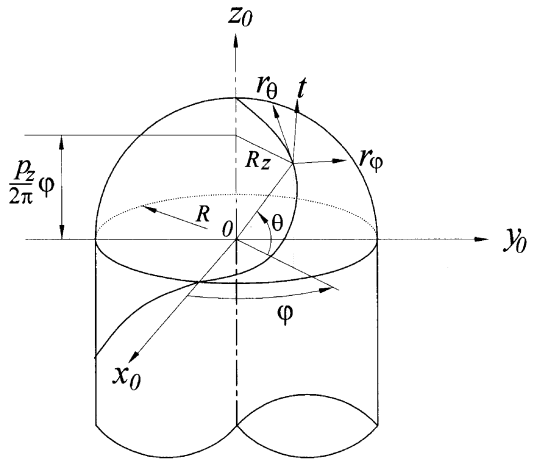


Fig. 1. Cutting edge of ball-end cutter.

where $0 \leq \varphi \leq \tan\beta_0, k = 1/\tan\beta_0$ and $\beta_0$ is the initial helix angle.

Thus, the normal helix cutting edge on the ball surface can be expressed as

$$\mathbf{r} = [r_x \quad r_y \quad r_z \quad 1]^T = \left[RC\varphi\sqrt{1-(k\varphi)^2} \quad RS\varphi\sqrt{1-(k\varphi)^2} \quad Rk\varphi \quad 1\right]^T. \tag{4}$$

As a result, the unit tangent vector, $\mathbf{t}$, is given by

$$\mathbf{t} = \frac{1}{\sqrt{(1-(k\varphi)^2)^2+k^2}}\left[(k^2\varphi^2 S\varphi - k^2\varphi C\varphi - S\varphi) - (k^2\varphi^2 C\varphi + k^2\varphi S\varphi - C\varphi)k\sqrt{1-(k\varphi)^2}0\right]^T. \tag{5}$$

The helix angle is the angle between the tangential vector of the helix and the tangential vector of the longitudinal axis of the ball surface $(r_\theta)$. In other words, the helix angle can be obtained via the following dot product:

$$C\beta = \frac{\mathbf{t}\cdot\mathbf{r}_\theta}{\|\mathbf{t}\|\,\|\mathbf{r}_\theta\|}, \tag{6}$$

where

$$\mathbf{r}_\theta = \frac{\partial \mathbf{r}}{\partial \theta} = [-RS\theta C\varphi \quad -RS\theta S\varphi \quad RC\theta \quad 0]^T.$$

From Eq. (6) the helix angle on the ball surface can be simplified as

$$\beta = C^{-1}\left(\frac{k}{\sqrt{(1-k^2\varphi^2)^2+k^2}}\right). \tag{7}$$

## 3. RAKE FACE MATHEMATICAL MODEL

This section derives a mathematical model for producing the helical cutting edge on the rake face of a ball-end cutter with a constant normal rake angle $\gamma_n$ using a conical grinding wheel.

Referring to Fig. 2, the coordinates of any point on line $\overline{p_o p_i}$ can be expressed in terms of coordinate system $(xyz)_2$ as follows:

$${}^2S = \begin{bmatrix} R\sqrt{C^2(\varepsilon+\varphi)+k^2\varphi^2S^2(\varepsilon+\varphi)} - \ell C\Omega_1 \\ R\sqrt{1-(k\varphi)^2}S(\varepsilon+\varphi) - \ell S\Omega_1 \\ 0 \\ 1 \end{bmatrix}, \tag{8}$$

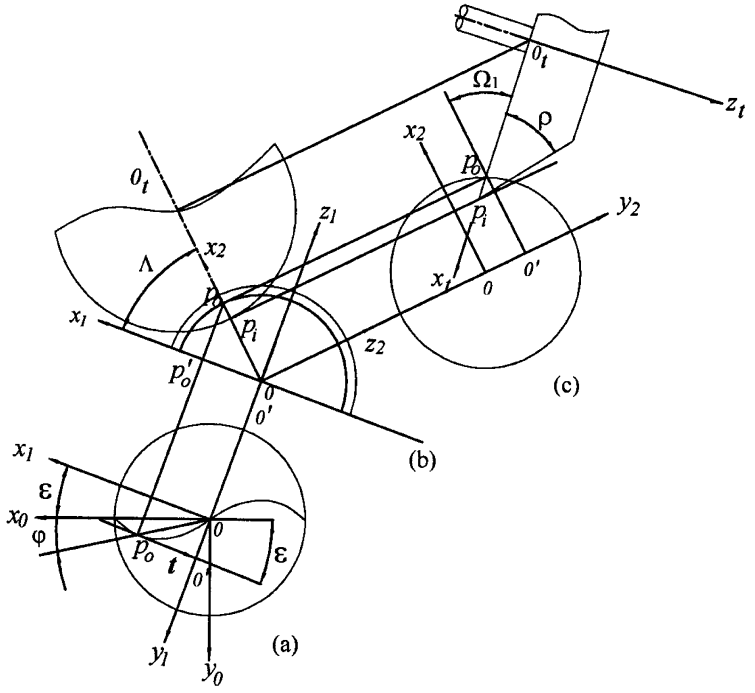


Fig. 2. Coordinate systems of interest when grinding rake surface of ball-end cutter.

where $\ell$ is the grinding depth, i.e., the distance between points $p_o$ and $p_i$. The grinding depth varies as the following function of the longitudinal angle $\varphi$:

$$\ell = \delta_{\max} + \delta_0 - \delta_0 \left( \frac{\delta_{\max}}{\delta_0} \right)^{k\varphi}, \tag{9}$$

where $\delta_0$ and $\delta_{\max}$ are the minimum and maximum grinding depths, respectively.

The pose of the grinding wheel with respect to frame $(xyz)_2$ can be expressed as

$${}^2A_t = \text{Trans}(\lambda_1, \lambda_2, 0)\text{Rot}(z, \Omega_1)\text{Trans}(\lambda_3, 0, 0)\text{Rot}(z, 180), \tag{10}$$

where

$$\lambda_1 = \overline{0'p_0} = R\sqrt{C^2(\varepsilon+\varphi) + k^2\varphi^2 S^2(\varepsilon+\varphi)}, \quad \lambda_2 = \overline{00'} = R_z S(\varepsilon+\varphi) = R\sqrt{1-(k\varphi)^2}S(\varepsilon\varphi),$$

and

$$\lambda_3 = \overline{0_t p_0} = (R_1 - \ell).$$

Equation (10) can be expressed in the following matrix form:

$${}^2A_t = \begin{bmatrix} -C\Omega_1 & 0 & -S\Omega_1 & \lambda_3 C\Omega_1 + \lambda_1 \\ -S\Omega_1 & 0 & C\Omega_1 & \lambda_3 S\Omega_1 + \lambda_2 \\ 0 & 1 & 0 & 0 \\ 0 & 0 & 0 & 1 \end{bmatrix}. \tag{11}$$

In order to grind the rake face, it is necessary to define the configuration of the tool frame $(xyz)_t$ relative to the ball-end cutter frame $(xyz)_0$, i.e.,

$$
\begin{aligned}
{}^0A_t &= {}^0A_1^1A_2^2A_t = \mathrm{Rot}(z_0,-\varepsilon)\mathrm{Rot}(y_1,-\Lambda)\ {}^1A_2 \qquad (12)\\
&= \begin{bmatrix}
-C\varepsilon C\Lambda C\Omega_1 - S\varepsilon S\Omega_1 & -C\varepsilon S\Lambda & -C\varepsilon C\Lambda S\Omega_1 + S\varepsilon C\Omega_1 \\
S\varepsilon C\Lambda C\Omega_1 - C\varepsilon S\Omega_1 & S\varepsilon S\Lambda & S\varepsilon C\Lambda S\Omega_1 + C\varepsilon C\Omega_1 \\
-S\Lambda C\Omega_1 & C\Lambda & -S\Lambda S\Omega_1 \\
0 & 0 & 0
\end{bmatrix}\\
&\quad \begin{bmatrix}
[(R_1-\ell)(C\Omega_1 + R\sqrt{C^2(\overline{\varepsilon+\varphi}) + k^2\varphi^2S^2(\varepsilon+\varphi)]C\varepsilon C\Lambda + [(R_1-\ell)S\Omega_1 + R\sqrt{1-\overline{(k\varphi)^2S(\varepsilon}+\varphi)]S\varepsilon \\
-[(R_1-\ell)C\Omega_1 + R\sqrt{C^2(\varepsilon+\varphi) + k^2\varphi^2S^2(\varepsilon+\varphi)]S\varepsilon C\Lambda + [(R_1-\ell)S\Omega_1 + R\sqrt{1-(k\varphi)^2}S(\varepsilon+\varphi)]C\varepsilon \\
[(R_1-\ell)C\Omega_1 + R\sqrt{C^2(\varepsilon+\varphi) + k^2\varphi^2S^2(\varepsilon+\varphi)]S\Lambda \\
1
\end{bmatrix}
\end{aligned}
$$

The rake face can be expressed in the ball-end cutter frame $(xyz)_0$ via the following coordinate transformation:

$$
\begin{aligned}
{}^0S &= {}^0A_1^1A_2^2S \qquad (13)\\
&= \begin{bmatrix}
-S\varepsilon C\Lambda[R\sqrt{C^2(\varepsilon+\varphi) + k^2\varphi^2S^2(\varepsilon+\varphi)} - \ell C\Omega_1] + S\varepsilon[R\sqrt{1-(k\varphi)^2}S(\varepsilon+\varphi) - \ell S\Omega_1 \\
-S\varepsilon C\Lambda[R\sqrt{C^2(\varepsilon+\varphi) + k^2\varphi^2S^2(\varepsilon+\varphi)} - \ell C\Omega_1] + C\varepsilon[R\sqrt{1-(k\varphi)^2}S(\varepsilon+\varphi) - \ell S\Omega_1 \\
S\Lambda[R\sqrt{C^2(\varepsilon+\varphi) + k^2\varphi^2S^2(\varepsilon+\varphi)} - \ell C\Omega_1] \\
1
\end{bmatrix}.
\end{aligned}
$$

It is noted in Eq. (13) that three angular parameters ($\varepsilon, \Lambda$ and $\Omega_1$) are undetermined. Parameter $\varepsilon$ at point $p$ between the tangent vector of the cutting edge and the $x_0$ axis is given as

$$
\cos\left(\frac{\pi}{2} - \varepsilon\right) = \frac{\mathbf{t}\cdot y_0}{\|\mathbf{t}\|\,\|y_0\|} = -\frac{(k^2\varphi^2C\varphi + k^2\varphi S\varphi - C\varphi)}{\sqrt{(1-(k\varphi)^2)^2 + k^2}}. \qquad (14)
$$

Equation (14) can be simplified as

$$
\varepsilon = S^{-1}\left(-\frac{(k^2\varphi^2C\varphi + k^2\varphi S\varphi - C\varphi)}{\sqrt{(1-(k\varphi)^2)^2 + k^2}}\right). \qquad (15)
$$

In Fig. 2a, segments $\overline{0p_0}, \overline{00'}$ and $\overline{0'p_0}$ have lengths of $R_z, R_zS(\varepsilon+\varphi)$ and $\sqrt{R^2 - \overline{00'}^2}$, respectively. Thus, parameter $\Lambda$ in Eq. (13) can be determined via the relationship

$$
\overline{0p_0}C(\varepsilon+\varphi) = \overline{0'p_0}C\Lambda. \qquad (16)
$$

In other words, parameter $\Lambda$ can be expressed as

$$
\Lambda = C^{-1}\left(\frac{\sqrt{1-(k\varphi)^2}C(\varepsilon+\varphi)}{\sqrt{C^2(\varepsilon+\varphi) + (k\varphi)^2S^2(\varepsilon+\varphi)}}\right). \qquad (17)
$$

Note that the third underdetermined parameter in Eq. (13), i.e., the rotational angle $\Omega_1$, is derived in Section 5.

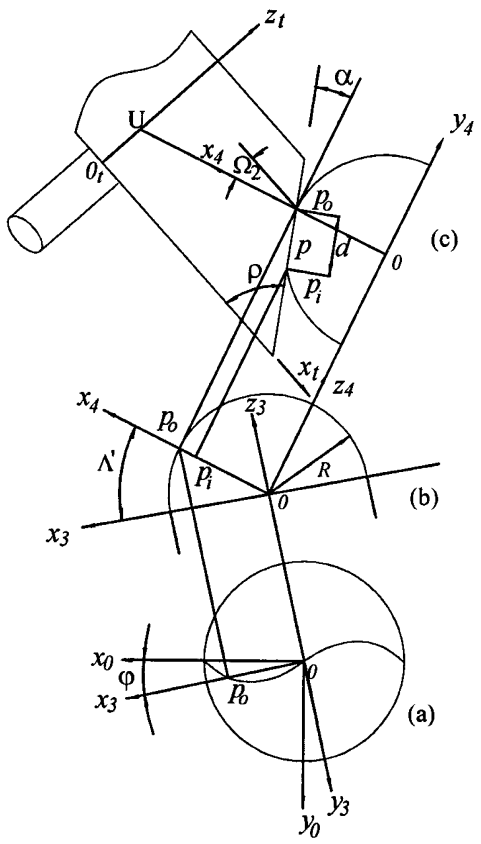


Fig. 3. Coordinate systems of interest when grinding rake surface of ball-end cutter.

## 4. FLANK FACE MATHEMATICAL MODEL

This section derives a mathematical model for producing the flank face of a ball-end cutter with a constant clearance angle $\alpha$ using a conical grinding wheel.

Referring to Fig. 3, the pose of the grinding wheel with respect to frame $(xyz)_4$ can be expressed as

$$^4A_t = \text{Trans}(\lambda_1, 0, 0)\text{Rot}(z, \Omega_1)\text{Trans}(0, -\lambda_2, 0)\text{Rot}(x, -90). \tag{18}$$

As shown in Fig. 4, parameters $\lambda_1$ and $\lambda_2$ in Eq. (18) are given by the following trigonometric functions:

$$\lambda_1 = \overline{0U} = R + (R_1 - h\cot\rho)/C\Omega_2 \tag{19}$$

$$\lambda_2 = \overline{o_tU} = h - (R_1 - h\cot\rho)\tan\Omega_2 \tag{20}$$

To grind the flank face, it is necessary to define the configuration of the tool frame $(xyz)_t$ with respect to the ball-end cutter frame $(xyz)_0$, i.e.,

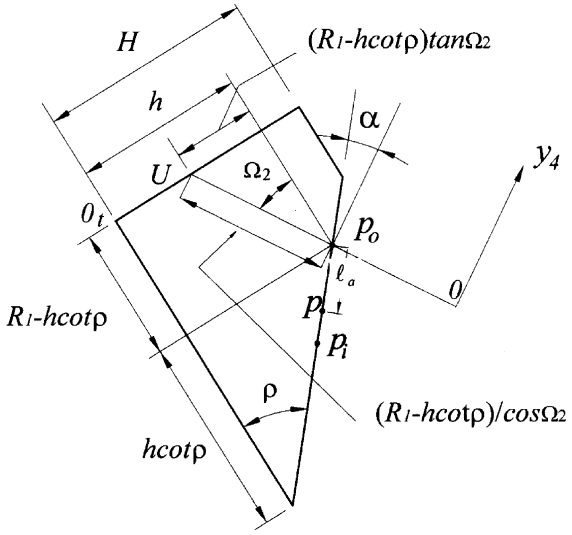


Fig. 4. Geometric relationships of interest when grinding flank surface of ball-end cutter.

$$
\begin{aligned}
{}^0A_t &= {}^0A_3^3A_4^4A_t = \mathrm{Rot}(z,\varphi)\mathrm{Rot}(y,-\theta)^3A_4 \qquad (21)\\
&= \begin{bmatrix}
-C\varphi C\theta C\Omega_2 + S\varphi S\Omega_2 & -S\varphi & C\varphi C\theta S\Omega_2 + S\varphi C\Omega_2 \\
-S\varphi C\theta C\Omega_2 - C\varphi S\Omega_2 & C\varphi & S\varphi C\theta S\Omega_2 - C\varphi C\Omega_2 \\
-S\theta C\Omega_2 & 0 & S\theta S\Omega_2 \\
0 & 0 & 0
\end{bmatrix}\\
&\quad \begin{bmatrix}
\left[(h-(R_1-h\cot\rho)\tan\Omega_2)S\Omega_2 + \left(R+\frac{(R_1-h\cot\rho)}{C\Omega_2}\right)\right]C\varphi C\theta + [(h-(R_1-h\cot\rho)\tan\Omega_2)]C\Omega_2 S\varphi \\
\left[(h-(R_1-h\cot\rho)\tan\Omega_2)S\Omega_2 + \left(R+\frac{(R_1-h\cot\rho)}{C\Omega_2}\right)\right]S\varphi C\theta - [(h-(R_1-h\cot\rho)\tan\Omega_2)]C\Omega_2 C\varphi \\
\left[(h-(R_1 h\cot\rho)\tan\Omega_2)S\Omega_2 + \left(R+\frac{(R_1-h\cot\rho)}{C\Omega_2}\right)\right]S\theta \\
1
\end{bmatrix}
\end{aligned}
$$

where $C\theta = \sqrt{1-(k\varphi)^2}$ and $S\theta = k\varphi$

In Eq. (21) the clearance angle $\alpha$, rotational angle $\Omega_2$ and conical angle of the grinding wheel $\rho$ are related via the following expression:

$$\Omega_2 = \frac{\pi}{2} - \rho - \alpha. \qquad (22)$$

The coordinates of any point on line $\overline{p_o p_i}$ in Fig. 3 can be expressed as

$${}^4S = [R - \ell_a\ S\alpha - \ell_a \#C\alpha\ 0\ 1]^T, \qquad (23)$$

where $0 \le \ell_a \le d$, in which $d$ is the width of the flank surface

The flank surface of the ball-end cutter can be obtained in the ball-end cutter frame as follows:

$${}^0S = {}^0A_3^3A_4^4S = [C\varphi C\theta(R-\ell_a S\alpha) + S\varphi(\ell_a C\alpha)S\varphi C\theta(R-\ell_a S\alpha) - C\varphi(\ell_a C\alpha)S\theta(R-\ell_a S\alpha)\ 1]^T. \qquad (24)$$

(Note that readers with an interest in generating the NC equations required to produce specific ball-end cutters using a CNC tool-grinding machine are referred to Hsieh and Lin [7] for a detailed description.)

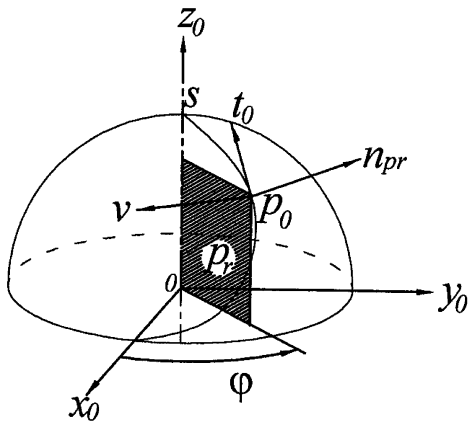


Fig. 5. Schematic illustration of cutting edge inclination angle.

## 5. CUTTING ANGLES

This section derives mathematical expressions for the cutting edge inclination angle, cutting edge angle and normal rake angle of the ball-end cutter considered in the preceding sections

The cutting edge inclination angle $(\lambda)$ is the angle between the unit tangent vector $\mathbf{t}$ of the cutting edge and the tool reference plane $p_r$ (see Fig. 5) and can be determined mathematically as follows:

$$\cos\left(\frac{\pi}{2}-\lambda\right) = \mathbf{t}\cdot\mathbf{n}_{pr}, \tag{25}$$

where $\mathbf{n}_{pr} = [-S\varphi\ C\varphi\ 0\ 0]^T$ is the normal vector of plane $p_r$.

The cutting edge angle $(\kappa_r)$ is the angle between the feed motion vector (i.e., the $z_0$ axis of the ball-end cutter frame $(\mathbf{x}yz)_O$) and the projection vector of the cutting edge on plane $p_r$. The cutting edge angle can be determined as

$$\cos\kappa_r = \frac{\mathbf{r}_\theta\cdot\mathbf{z}_0}{|\mathbf{r}_\theta|\,|\mathbf{z}_0|} = \sqrt{1-(k\varphi)^2}. \tag{26}$$

Points $p_o, p_i$ and $s$ in Fig. 6 can be expressed in coordinate system $(xyz)_2$ as follows:

$${}^2p_o = [\sqrt{R^2 - R_z^2S^2(\varepsilon+\varphi)}\ R_zS(\varepsilon+\varphi)\ 0\ 1]^T \tag{27}$$

$${}^2p_i][RS\Lambda\ 0\ RC\Lambda\ 1]^T \tag{28}$$

$${}^2p_i = [\sqrt{R^2 - R_z^2S^2(\varepsilon+\varphi)} - \ell C\Omega_1\ R_zS(\varepsilon+\varphi) - \ell S\Omega_1\ 0\ 1]^T. \tag{29}$$

Consequently, the normal vector of the reference plane $p_r$ is given by

$${}^2n_{pr} = [C\Lambda\ H\ -S\Lambda\ 0]^T, \tag{30}$$

where

$$H = \frac{-\sqrt{C^2(\varepsilon+\varphi)+(k\varphi)^2S^2(\varepsilon+\varphi)C\Lambda}}{\sqrt{1-(k\varphi)^2S(\varepsilon+\varphi)}}.$$

The direction of line $\overline{p_op_i}$ is given by (see Fig. 2)

$${}^2n_{L_i} = [\ell C\Omega_1 \quad \ell S\Omega_1 \quad 0 \quad 0]^T. \tag{31}$$

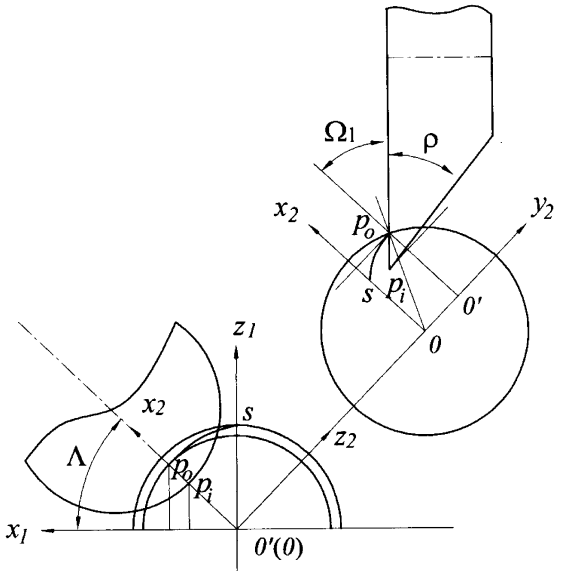


Fig. 6. Schematic illustration of normal rake angle.

By convention, the normal rake angle is defined as

$$C\left(\frac{\pi}{2}-\gamma_n\right)=\frac{|^2n_{pr}\cdot{}^2n_L|}{|^2n_{pr}|\,|^2n_L|}. \tag{32}$$

Substituting Eqs. (30) and (31) into (32), the normal rake angle $\gamma_n$ is obtained as

$$S\gamma_n=\left(\frac{C\Lambda C\Omega_1+HS\Omega_1}{\sqrt{1+H^2}}\right). \tag{33}$$

Assuming that $\gamma_n$ is a constant, the rotational angle $\Omega_1$ (i.e., the third underdetermined parameter in Eq. (13)) is determined by

$$\Omega_1=S^{-1}\left(\frac{\sqrt{1+H^2}S\gamma_n}{\sqrt{H^2+C^2\Lambda}}\right)-\tan^{-1}\left(\frac{C\Lambda}{H}\right). \tag{34}$$

## 6. NUMERICAL EVALUATION

In this study, the validity of the mathematical model developed in the previous sections was verified by means of numerical simulations using parameter settings of $R=6$, $\gamma_n=30^\circ$, and $\beta_0=30^\circ$ or $\beta_0=36^\circ$. As expected, Fig. 7 shows that the cutting edge inclination angle reduces from the bottom of the ball to the top of the ball. Meanwhile, Fig. 8 shows that the cutting edge angle increases from the bottom of the ball to the top of the ball. Observation of Figs. 7 and 8 shows that the effect of a higher value of $\beta_0$ has a larger cutting edge inclination angle and a small cutting edge angle, respectively.

## 7. CONCLUSIONS

This paper has developed a general mathematical model of a ball-end cutter. In developing the model, it has been assumed that the rake face has a constant normal rake angle and the flank face has a constant orthogonal clearance angle. Mathematical expressions for the pose of the grinding wheel with respect to the workpiece

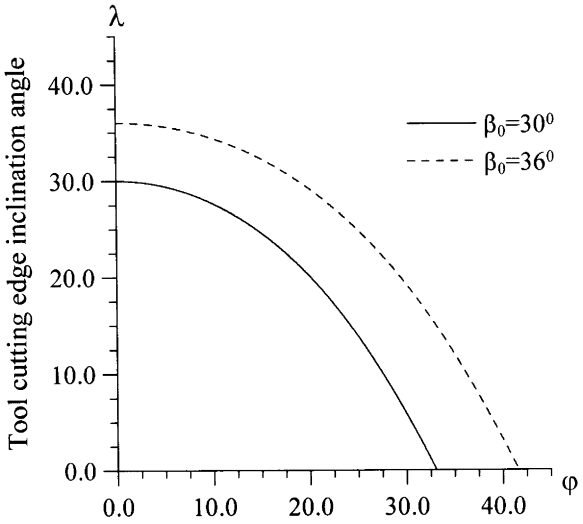


Fig. 7. Variation of cutting edge inclination angle along cutting edge.

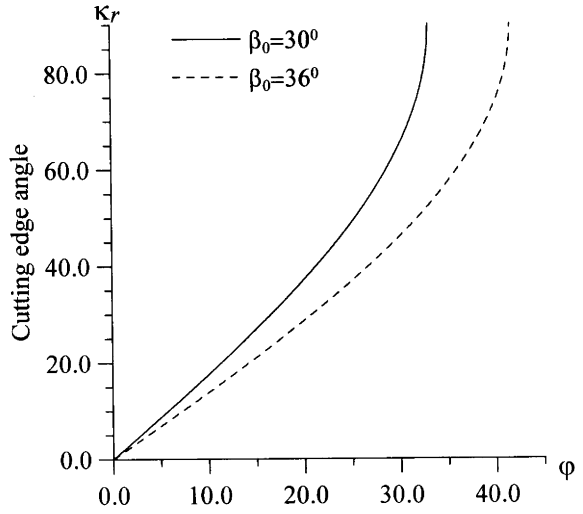


Fig. 8. Variation of cutting edge angle along cutting edge.

during the grinding process have also been derived. Thus, the methodology presented in this study provides a suitable basis for deriving the NC equations required to machine specific ball-end cutters using a CNC tool-grinding machine.

## ACKNOWLEDGEMENT

The author gratefully acknowledges the financial support provided to this study by the National Science Council of Taiwan under Grant No. NSC100-2221-E-269-009.

## REFERENCES

1. Milfellner, M. and Cus, F., "Simulation of cutting forces in ball-end milling", *Robotics & Computer-Integrated Manufacturing*, Vol. 19, pp. 99–107, 2003.
2. Lu, Y. Takeuchi, Y. Takahashi, I. and Anzai, M., "An integrated system development for ball end mill design,

creation and evaluation", *International Journal of Advanced Manufacturing Technology*, Vol. 25, pp. 628–646, 2005.
3. Jin, M., Goto, I., Watanabe, T., Kurosawa, J., and Murakawa, M., "Development of CBN ball-nosed end mill with newly designed cutting edge", *Journal of Materials Processing Technology*, Vol. 192–193, pp. 48–54, 2007.
4. Xiong, F. and Bin, H., "CNC rake grinding for a taper ball-end mill with torus-shaped grinding wheel", *International Journal of Advanced Manufacturing Technology*, Vol. 21, pp. 549–555, 2003.
5. Chen, F. and Bin, H., "A novel CNC grinding method for the rake face of a taper ball-end mill with a CBN spherical grinding wheel", *International Journal of Advanced Manufacturing Technology*, Vol. 41, pp. 846–857, 2009.
6. Chen, F.J., Yin, S.H and Hu, S. J., "Modeling and computer simulation of grinding for ball-end milling cutter with equal normal rake angle", *Advanced Materials Research*, Vol. 53–54, pp. 225–230, 2008.
7. Hsieh, J.-F. and Lin, P. D., "Production of multifluted drills on six-axis CNC tool-grinding machine", *International Journal of Machine Tools & Manufacture*, Vol. 43, pp. 1117–1127, 2003.